J. Biomed. Eng. Res : 713-720, 2007

Automatic Bone Segmentation from CT Images Using Chan-Vese Multiphase Active Contour

P. T. H. Truc[1], T.-S. Kim[2], Y. H. Kim[3], Y. B. Ahn[4], Y. K. Lee[1], S. Y. Lee[1]

[1]*Department of Computer Engineering,* [2]*Department of Biomedical Engineering,*
[3]*College of Advanced Technology, Kyung Hee University, Yongin, Kyungki, Republic of Korea,*
[4]*Department of Electronic Engineering, Konkuk University*
(Received April 2, 2007. Accepted August 16, 2007)

Abstract

In image-guided surgery, automatic bone segmentation of Computed Tomography (CT) images is an important but challenging step. Previous attempts include intensity-, edge-, region-, and deformable curve-based approaches [1], but none claims fully satisfactory performance. Although active contour (AC) techniques possess many excellent characteristics, their applications in CT image segmentation have not worthily exploited yet. In this study, we have evaluated the automaticity and performance of the model of Chan-Vese Multiphase AC Without Edges towards knee bone segmentation from CT images. This model is suitable because it is initialization-insensitive and topology-adaptive. Its segmentation results have been qualitatively compared with those from four other widely used AC models: namely Gradient Vector Flow (GVF) AC, Geometric AC, Geodesic AC, and GVF Fast Geometric AC. To quantitatively evaluate its performance, the results from a commercial software and a medical expert have been used. The evaluation results show that the Chan-Vese model provides superior performance with least user interaction, proving its suitability for automatic bone segmentation from CT images.

Key words : bone segmentation, active contours, level set methods, CT images.

I. INTRODUCTION

Recently, due to increasing computing power, computer-aided surgery planning or image-guided surgery systems become popular in clinical procedures. In computer-assisted orthopedic surgery, image segmentation, especially bone segmentation from CT imagery, is a critical component but a challenging task due to i) inhomogeneous bone structures and ii) low contrast edges. Inhomogeneous regions are due to the nature of bone structure in which the outer layer (i.e., cortical bone) is denser than the inner one (i.e., spongy bone). As a result, the cortical bone appears brighter in CT images while the spongy bone is darker and sometimes textured. Moreover, during image acquisition process, small gaps can exist in the bone surfaces where blood vessels gothrough. Also, when the boundaries of two bone regions are close to each other, they tend to be diffused making the background pixels between them brighter and thus contrast lower. The boxes in Fig. 1 indicate these challenging characteristics.

Some research packages including ANALYZE [2], VTK [3], and Insight Toolkit ITK [4] are available for medical image processing in general and segmentation in particular. Most segmentation processes, which utilize these packages, use a simple threshold and initial boundaries, get the resulting contours, and connect the discontinued segments with linear lines. These approaches have two major disadvantages. One is that visual inspection of every single image is needed for proper settings of the threshold value. The other is that some regions of image noise having high intensity are misclassified as bone and some bone regions which are blurred and resemble background will usually be omitted. Therefore, it is desirable to develop automatic segmentation techniques that

This work was supported by grant (R01-2006-000-11209-0) from the Basic Research Program of the Korea Science & Engineering Foundation.
This research was supported by the MIC (Ministry of Information and Communication), Korea, under the ITRC (Information Technology Research Center) support program supervised by the IITA (Institute of Information Technology Advancement) (IITA-2006-(C1090-0602-0002)).
Corresponding Author : Tae-Seong Kim, Ph.D.
Functional and Metabolic Imaging Center, Department of Biomedical Engineering, Kyung Hee University.
1 Seocheon-dong, Giheung-gu, Yongin-si, Gyeonggi-do, Republic of Korea, 446-701.
Tel : +82-31-201-3731 / Fax : +82-43-201-3666
E-mail: tskim@khu.ac.kr

both improve segmentation performance and reduce user interactions. There have been a few attempts including global thresholding, region growing, region competition, watershed segmentation, etc. as surveyed in [1] and [5]. Unfortunately, none of them claims full automaticity and less user interactivity for bone segmentation according to the criteria mentioned above.

Recently, active contour (AC)-based segmentation techniques are being actively researched and developed. Since it was first introduced by Kass [6] in 1988, AC model (a.k.a. snakes) has attracted much attention in the image segmentation research community. To date, there are two types of AC models in literature: parametric AC's (e.g. [6-8]) and geometric AC's (e.g. [9-12]). In general, AC models are the descriptions of contours in 2D or surfaces in 3D which evolve under an appropriate energy to move toward desired features, such as object boundaries. The parametric AC's, which depend on the parameterizations of the contours, are driven to seek the minimal energy state while the geometric ones are evolved by the level-set framework [13-14] in which they are implicitly represented by the zero level-set of a function.

In applications of AC models on CT bone segmentation, some research work have been done. They tried to modify the parametric AC's, which are edge-based, by incorporating region-based information as in [15-16], [5] or optimizing the flow using the genetic algorithm as in [17]. Although those modified active contour models can be less sensitive to noise or can overcome the local minima problem, they are still far from automatic bone segmentation. By an automatic bone segmentation algorithm, we mean the algorithm that can correctly segment bone regions with minimal user interactions such as image-dependent initialization or prior information about bone shapes. To test the techniques, in this study, we have implemented five latest AC approaches: namely GVF AC [8], Geometric AC [9], Geodesic AC [10], GVF Fast Geometric AC [11], and Chan-Vese (CV) Multiphase AC Without Edges [12] and then built up a segmentation system utilizing each of these AC models to extract knee bones from CT data. According to the above categorization, the GVF AC model belongs to the parametric AC's whilst the other four are of the geometric ones. Our motivation here is to find the most appropriate technique for automatic bone extraction. These models are good candidates because of their salient characteristics such as initialization insensitiveness and automatic splitting and mergingability to capture multiple objects. Together with qualitative evaluations of these models' performances, suitable measures are used to compare their performances against the performance of a commercial software and a medical expert. Both qualitative and quantitative evaluations indicate that the CV Multiphase AC Without Edges model produces excellent segmentation results, proving that fully automatic bone segmentation could be possible.

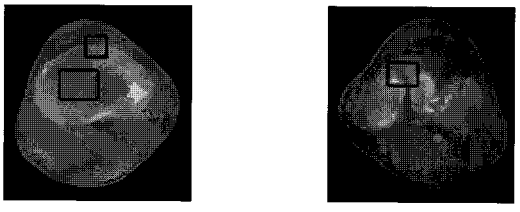

Fig. 1. Typical CT images showing bones with challenging characteristics in segmentation such as (a) gaps and texture areas and (b) weak edges.

II. MATERIALS AND METHODS

In this section, we first introduce the 3D-DOCTOR software: the commercial software for segmentation commonly used in the clinic. Then, we briefly describe the five AC models evaluated in this study. These models possess the following suitable features that make themselves good candidates for the automatic bone segmentation. The GVF AC is initialization insensitive and the geometric, geodesic, and GVF fast geometric AC models are adaptive to topology changes. The CV multiphase AC model has both of these advantages.

A. 3D-DOCTOR Software

3D-DOCTOR[1] (available from Able software Corp.) is a commercial software that is approved by FDA (US Food and Drug Administration with 510K clearance) for medical imaging and 3D visual- ization applications. It is currently being used by leading hospitals, medical schools, and research organizations around the world. For image segmentation, depending on the quality of images, 3D-DOCTOR provides different methods such as Fully Automatic Texture-based Segmentation, Thresholding-based Interactive Segmentation, Region-based Object Segm-entation, and Easy-to-use Polygon-based Manual Tracing.

Fully Automatic Texture-based Segmentation works well only for images with distinguishable texture, color, and contrast between objects. However, since CT images do not have such a good quality, we use Thresholding-based

1. website: http://www.ablesw.com/3d-doctor/

Interactive Segmentation to extract bone structures from CT images as follows. For every CT image, a trained expert interactively chooses a minimum and maximum threshold to demarcate the bone regions. All pixels within the minimum and maximum threshold range are labeled as bone while all others are regarded as background. Then, the boundaries of bone regions in the current image are extracted. The threshold values can be adjusted to obtain better results. The resultant boundary lines can be edited by the available "Edit" tools. Finally, the boundary data are saved. All these steps are repeated for other images.

B. Gradient Vector Flow Active Contour

The GVF [8] refers to the definition of slowly-varying and bidirectional external force that helps an active contour reach the object boundaries with a large capture range. One of its distinguished points is the ability to move into the boundary concavities. One can think of this flow field as optimal direction to be followed to locate the object boundaries.

In order to build up this field, an appropriate edge map function $g(x,y)$ having larger values near the image edges is first chosen. To this end, a Gaussian-derived function on the image gradient is usually considered for its smooth characteristic:

$$g(x,y) = 1 - \frac{1}{\sqrt{2\pi}\,\sigma_E} e^{-\frac{|\nabla (G_\sigma * I)(x,y)|^2}{2\sigma_E^2}} \tag{1}$$

where σ_E is variance and $[G_\sigma * I]$ is the convolution output of the input image with a Gaussian kernel.

The GVF is defined as a two-dimensional vector field $[u(x, y), v(x, y)]$, that minimizes the following energy functional

$$E(u,v) = \iint_\Omega \mu(u_x^2 + u_y^2 + v_x^2 + v_y^2) + |\nabla g|^2 |(u,v) - \nabla g|^2 \, dxdy$$

where u_x, u_y, v_x, and v_y are the spatial derivatives of the field and μ a noise-control parameter.

This functional keeps the GVF field nearly same as the gradient of the edge map, ∇g, in the neighborhood of the boundaries where $|\nabla g|$ is large. At the same time, the field still has significant values in the homogeneous regions, where $|\nabla g|$ gets close to 0, via a diffusion process. One can optimize $[u(x, y), v(x, y)]$ using the gradient descent method and the calculus of variations

$$\begin{aligned} \frac{du}{dt} &= \mu \nabla^2 u - (u - g_x)|\nabla g|^2 \; ; \\ \frac{dv}{dt} &= \mu \nabla^2 v - (v - g_y)|\nabla g|^2 \end{aligned} \tag{2}$$

where g_x and g_y are the spatial derivatives of g.

In [8], a parametric AC using the normalized GVF (NGVF) $[\hat{u} = u/\sqrt{u^2+v^2}\,,\ \hat{v} = v/\sqrt{u^2+v^2}\,]$ was proposed for boundary extraction in the following way:

$$C_t(p) = \alpha \frac{\partial^2 C}{\partial p^2}(p) - \beta \frac{\partial^4 C}{\partial p^4}(p) + [\hat{u}(p), \hat{v}(p)] \tag{3}$$

where $C(p) = [x(p), y(p)] : [0, 1] \rightarrow R^2$ is the parameterized curve, and α and β the adjustment constants. The first two terms of this flow are for regularization and the last one, the NGVF, is served as an external force pulling the curve toward the object's boundaries.

Such a flow depends on the parameterizations of the curve and cannot topologically change to track multiple objects. Also it involves the second and fourth order derivatives that are difficult to estimate. It is, however, relatively free of the initial conditions due to the GVF's characteristics mentioned above.

C. Geometric AC and Geodesic AC

Geometric active contours [9], [18] are based on the theory of curve evolution [19] and the level set method [14]. In this framework, curves C are represented by the zero level set of a Lipschitz function $\varnothing(x, y; t)$ and their evolutions are performed using only geometric measures, making themselves independent of the curves' parameterizations.

Toward the construction of the flow, a signed distance function is used:

$$\begin{cases} C = \{(x,y) : \varnothing(x,y) = 0\}, \\ inside(C) = \{(x,y) : \varnothing(x,y) > 0\}, \\ outside(C) = \{(x,y) : \varnothing(x,y) < 0\}. \end{cases} \tag{4}$$

The Geometric AC flow evolves $\varnothing$ according to

$$\varnothing_t = g(\kappa + V_0)|\nabla \varnothing| \tag{5}$$

where κ is the Euclidean curvature, V_0 a constant, and $g \equiv g(\vec{x}) = e^{-\frac{1}{2}|\nabla G_\sigma(\vec{x}) * I(\vec{x})|^2}$ an edge-based function.

In (5), the curvature κ-based flow has the properties of

smoothing the curve, while V_0 shrinks or expands the contour along its normal direction at a constant velocity. The product $g \cdot (\kappa + V_0)$ determines the overall evolution speed of level sets of $\varnothing(x, y; t)$. At the same time, the main use of g has the effect of stopping the curve when it reaches to the object boundaries.

In contrast to the parametric AC's, the geometric flow is topology independent and thus allows the AC to detect multiple objects. This scheme works well in general for objects that have good contrast. In cases where there are high variations of gradient as well as gaps along the edge, this contour, however, tends to pass through the object boundaries. To overcome this limitation, the following evolution flow, called the geodesic AC flow, was introducedin [10], [20] and can be expressed as

$$\varnothing_t = g(\kappa + V_0)|V\varnothing| + \nabla g \cdot \nabla \varnothing . \tag{6}$$

Comparing against the old model given in (5), we see that the extra stopping term $(\nabla g \cdot \nabla \varnothing)$ is used to increase the attraction of the evolving contour toward the boundaries.

D. GVF Fast Geometric AC

Inspired from the observations that the NGVF consists of the optimal direction to be followed to reach the object boundaries and that evolving the contour in the direction of its normal is a main characteristic of the geometric active contour flow, Paragios et al. [11] proposed an integration of NGVF into the geometric AC:

$$\begin{aligned}\varnothing_t(p) = g \cdot \{[H(p) + \beta\kappa]|\nabla \varnothing(p)| - \\ [1 - |H(p)|][\hat{u}, \hat{v}] \cdot \nabla \varnothing(p)\end{aligned} \tag{7}$$

where $H(p) = sign([\hat{u}, \hat{v}] \cdot N(p))e^{-\delta|[\hat{u}, \hat{v}] \cdot N(p)|}$, with δ a scale factor has significant values when the normal and the NGVF are close to orthogonal.

In the above flow, the use of has the effect of regularizing the propagation, and the use of $[1 - |H(p)|][\hat{u}, \hat{v}] \cdot \nabla \varnothing(p)$ has the effect of a bidirectional flow that moves the curve toward object boundaries from either sides, while the remaining term $H(p)|\nabla \varnothing|$ has the effect of an adaptive balloon force used to determine the evolution when the bidirectional flow term becomes inactive. Similar to that of the geometric AC, the overall speed of this curve evolution is coupled with the edge-driven information via a stopping term g.

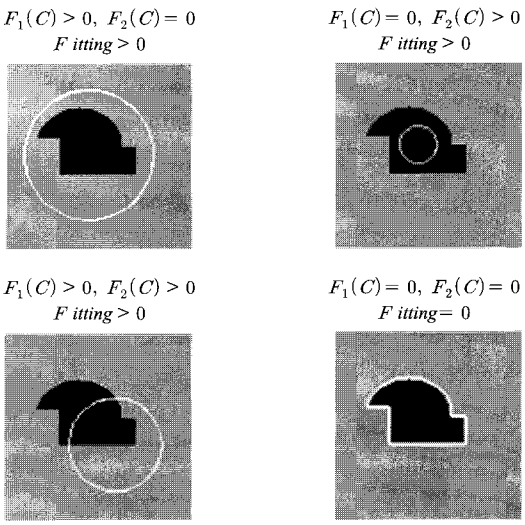

Fig. 2. All possible positions of the curve. When it is on the boundary of the object, the "fitting" term is minimized.

E. Chan-Vese Multiphase AC Without Edges

Chan and Vese proposed in [21] an alternative form of AC, called the AC without edges (shortly, the CV AC model), based on the Mumford and Shah functional for segmentation [22] and the level set framework [14]. Unlike other level set-based AC's which rely on the gradient of the image as the stopping term and thus have unsatisfactory performance in noisy images, the CV model does not use the edge information (so named "without edges") but utilizes the difference between the regions inside and outside of the curve.

In this case, the image u_0 is assumed to be consisted of two areas with approximately piecewise- constant intensities, of different value c_{in} and c_{out}. The "fitting" term is defined as:

$$\begin{aligned}F_1(C) + F_2(C) = \int_{inside(C)} |u_0(x, y) - c_1|^2 dxdy \\ + \int_{outside(C)} |u_0(x, y) - c_2|^2 dxdy\end{aligned} \tag{8}$$

where c_1 and c_2 are respectively the average intensities inside and outside the variable curve C.

As can be seen in Fig. 2, the "fitting" term is minimized if the curve C is placed exactly on the boundary of the two areas.

The level set formulation of this model is expressed as:

$$\varnothing_t = |\nabla \varnothing|[\nu\kappa - (u_0 - c_1)^2 + (u_0 - c_2)^2] \tag{9}$$

where ν is a smoothing constant.

This flow evolves the AC, looking for a two-phase segmentation of the image, given by $u(x,y) = c_{in}\ H[(x,y)]$

$+c_{out}(1-H[\varnothing(x,y)])$, where H is the Heaviside function:

$$H(z)=\begin{cases}1, & \text{if } z\geq 0,\\ 0, & otherwise.\end{cases} \tag{10}$$

The main advantages of the CV snake over other active contour models are i) it automatically detects interior contours and ii) the initial curve can be placed anywhere in the image.

For multiphase cases, we can write illustratively the formulations for four phases or classes (and therefore using the two level sets functions $\varnothing_1$ and $\varnothing_2$) as

$$\frac{\partial\varnothing}{\partial t}=|\nabla\varnothing_1|\left\{\nu.div\left(\frac{\nabla\varnothing_1}{|\nabla\varnothing_1|}\right)-\left[(u_0-c_{11})^2-(u_0-c_{01})^2\right]H(\varnothing_2)\right.$$
$$\left.-\left[(u_0-c_{10})^2-(u_0-c_{00})^2\right](1-H(\varnothing_2))\right.$$
$$\frac{\partial\varnothing}{\partial t}=|\nabla\varnothing_2|\left\{\nu.div\left(\frac{\nabla\varnothing_2}{|\nabla\varnothing_2|}\right)-\left[(u_0-c_{11})^2-(u_0-c_{10})^2\right]H(\varnothing_1)\right.$$
$$\left.-\left[(u_0-c_{10})^2-(u_0-c_{00})^2\right](1-H(\varnothing_1))\right.$$

where

$$c_{11}(\varnothing)=average(u_0)\,in\{(x,y):\ \varnothing_1(x,y)>0,\ \varnothing_2(x,y)>0\},$$
$$c_{10}(\varnothing)=average(u_0)\,in\{(x,y):\ \varnothing_1(x,y)>0,\ \varnothing_2(x,y)<0\},$$
$$c_{01}(\varnothing)=average(u_0)\,in\{(x,y):\ \varnothing_1(x,y)<0,\ \varnothing_2(x,y)>0\},$$
$$c_{00}(\varnothing)=average(u_0)\,in\{(x,y):\ \varnothing_1(x,y)<0,\ \varnothing_2(x,y)<0\}.$$

III. RESULTS AND DISCUSSIONS

In this section, the performance of the CV multiphase AC without edges model is compared against those of other four approaches and the commercial 3D-DOCTOR software. To do so, we apply all five techniques and the 3D-DOCTOR software on a set of fifteen CT images covering the knee regions of one person. The evaluation includes both qualitative and quantitative comparisons of the obtained results.

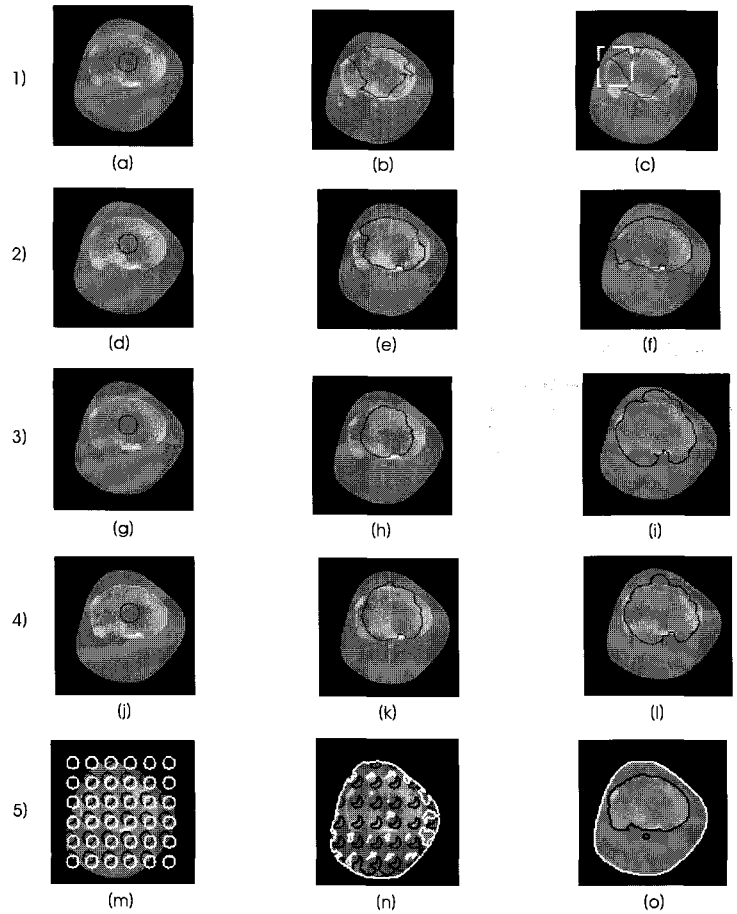

Fig. 3. CT bone segmentation results using GVF AC (row 1), GVF Fast Geometric AC (row 2), Geometric AC (row 3), Geodesic AC (row 4), and CV AC (row 5). From left to right: the initial contour, the intermediate evolving contour, and the final contour. The CV AC model generates the best segmentation results among the five methods considered.

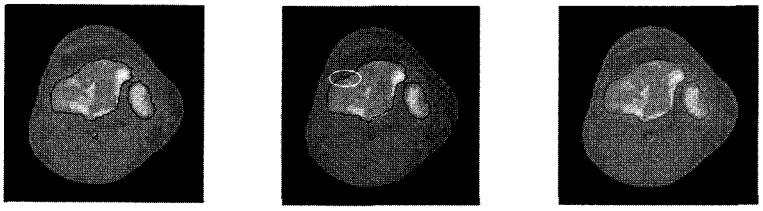

(a) (b) (c)

Fig. 4. Qualitative comparison. (a) Segmentation result from the CV multi-phase AC without edges model, (b) the 3D- DOCTOR software, and (c) the expert manual delineation. The CV AC does not contain impractically cross-over parts while the contour from the 3D-DOCTOR software does (indicated by the white ellipse).

A. Qualitative Evaluation

For qualitative evaluation, we considered the segmentation to be satisfactory if the AC correctly finds the bone boundaries as determined visually. However, unsatisfactory if the AC does not converge to correct boundaries.

The evolving AC will stop when the relative difference in areas of segmented regions between two consecutive iterations is less than 0.1 percent, i.e.,

$$\frac{|A_k - A_{k-1}|}{A_k} < 0.1\% \tag{11}$$

where A_k and A_{k-1} are respectively the areas of segmented regions in iteration k^{th} and $(k-1)^{th}$.

Fig. 3 shows segmentation results obtained using the five mentioned AC models. For the first four models: GVF, GVF Fast Geometric, Geometric, and Geodesic AC's, we initialize the contours inside the bone regions because the outside-initialized contours tend to stop at the outer boundary and can never evolve toward the inner one as expected. One may think of using a threshold to set the initial contours. However, for the level set-based AC's, it is easier to set the contours geometrically due to the signed distance function (4) although arbitrary initial boundaries by a threshold will work as well. Moreover, to select a threshold suitable for a set of images is not an easy problem.

These four models cannot correctly extract bone structures because of their limitations in noisy environment. As shown in Fig. 3 - row 1, the lower left part of the GVF snake after a certain number of iterations could not propagate anymore because the NGVF in that area is close to orthogonal to the inward normal of the curve. This is plausible when dealing with noisy images where some noise can be accidentally considered as linesegments. To remove such noise, the Gaussian-derived edge map function (1) should be more desirable, but it in turn can smooth the edges as well. In this situation, the balloon force in the GVF fast geometric AC model (7) can help to overcome this limitation (Fig. 3(e)). However, as shown in Fig. 3(f) it tends to pass through and thus cannot stop at the desired but weak edges. The geometric AC model (Fig. 3 - row 3) also suffers from the same problem of the GVF fast geometric AC. On the other hand, comparing Fig. 3(l) with (i), we can see that the geodesic AC (row 4) with the extra stopping term (6) can pull back the boundary-passing-through contour. Nevertheless, this term is still not strong enough at some blurred parts of the boundary.

Differently, the CV AC model can successfully find the bone boundaries as shown in Fig. 3 - row 5. In this experiment, two level set functions (i.e., four phases) is enough to catch all objects because the maximum number of bone regions in the dataset is three. This model works well in this case because it is not based on the edge function to stop the evolving contour on the desired boundary which is really blurred. Carefully observing Fig. 3(o), we can see that the small bone region (the small contour under the bigger one) is also detected without any prior information. In order to detect this region in case of using the other four models, we need to create an initial contour in its neighborhood, which obviously requires much user interaction. One other interesting thing is that it has a robust initialization scheme in which many small contours are initially placed such that they cover the whole image (Fig. 3(m)). With this scheme, the contours can converge to desired object boundaries no matter where they are.

The qualitative comparisons between the results from the CV AC model and those from the 3D- DOCTOR software are presented in Fig. 4. The CV AC model yields better results in the sense that it is smoother and does not contain impractically sophisticated parts as the commercial software does. We can see clearly from Fig. 4(b) that the commercial software sometimes generates cross-over contours which of course cannot truthfully represent any real bone structure.

B. Quantitative Evaluation

Qualitative evaluation in the previous section shows that the

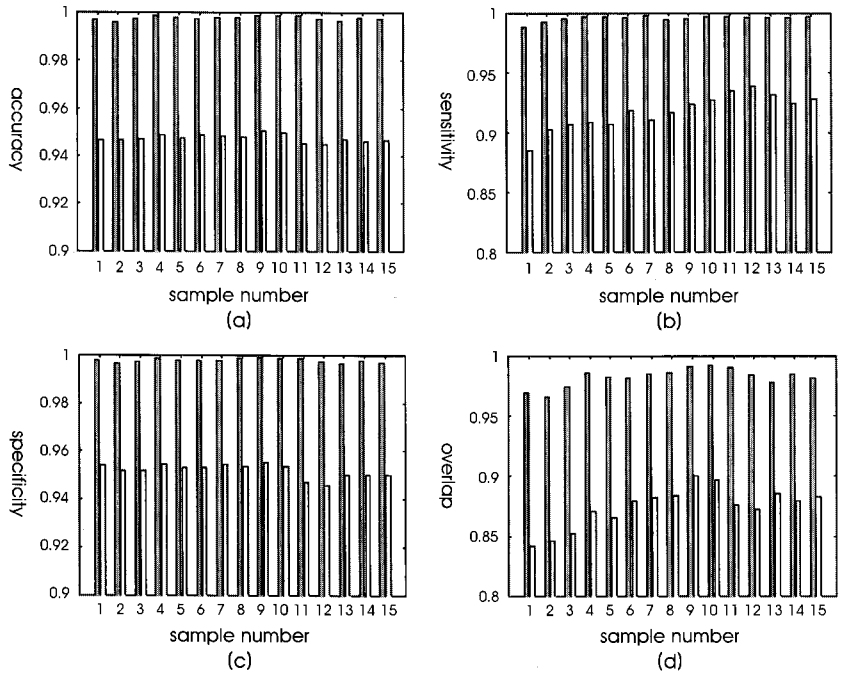

Fig. 5. Performance plots vs. sample number: (a) accuracy, (b) sensitivity, (c) specificity, and (d) overlap. Left dark bars: the CV AC model; right bright bars: the commercial software. The mean and SD of these measurements are given in Table I.

first four models fail to converge. Obviously their performances are worse than that of the CV AC model. Therefore, in this section, we validate the performance of this model in comparison with the commercial software only. To this end, the expert manual delineations are used as the "ground truth" and the "goodness" measures such as accuracy, sensitivity, specificity, and overlap introduced in [23] are adopted. These measures are computed on a pixel-wise manner, in which bone-labeled pixels are considered positive and background pixels negative. Compared with the "ground truth", let TP be the number of pixels true positive (correctly classified as objects), TN true negative (correctly classified as background), FP false positive (background misclassified as objects), and FN false negative (objects misclassified as background). Then, we have:

$$accuracy = \frac{TP+TN}{TP+FP+TN+FN};\quad sensitivity = \frac{TP}{TP+FN};$$

$$specifictity = \frac{TN}{TN+FP};\quad overlap = \frac{TP}{TP+FP+FN}.$$

For every sample slice in the dataset, the accuracy, sensitivity, specificity, and overlap measures are calculated from the segmentation results of the CV AC model and of the 3D-DOCTOR software, both compared against the "ground truth". These performance measures for the whole dataset are presented in Fig. 5 and their mean and standard deviation (SD) are given in Table I. It can be seen that the CV AC model yields superior performance than the commercial software does. This is due to the fact that this model does not requires smoothing the initial image even if it is noisy and thus the objects' boundaries are accurately detected and preserved.

Ⅳ. CONCLUSION

We have examined the five different active contour-based

Table 1. The mean and standard deviation of the accuracy, sensitivity, specificity, and overlap measurements of the CA AC model and the commercial software.

Approach		accuracy	sensitivity	specificity	overlap
CV AC	Mean	0.9975	0.9957	0.9978	0.9822
	SD	8.E−4	25.E−4	9.E−4	76.E−4
Commercial	Mean	0.9475	0.9178	0.9521	0.8744
	SD	16.E−4	143.E−4	27.E−4	169.E−4

segmentation techniques, which can be categorized as the without-edge type (the CV AC model) and the edge-based type (the four other AC models). Both qualitative and quantitative evaluations have been performed by applying these techniques toward knee bone segmentation from a set of CT images. Qualitatively, the results showed that the edge-based AC's failed to detect correct boundaries of bone regions because they were highly sensitive to noise and low-contrast boundaries which are the characteristics of CT images. On the other hand, the CV AC model showed excellent potential in segmenting bone regions correctly and automatically with some advantages such as robustness in curve initialization and automatic detection of multiple objects. This model also generated visually better results than the commercial 3D-DOCTOR software did in the sense that its contours were smoother and did not contain cross-over parts which could not truthfully represent real bone structures.

For quantitative evaluation, performance measures such as accuracy, sensitivity, specificity, and overlap were calculated over the whole dataset, basing to the medical expert manual delineations as the "ground truth". The performance of the CV AC model was superior to that of the commercial software. Consequently, we consider that the CV Multiphase AC Without Edges model should be a preferred choice for the automatic bone segmentation work.

REFERENCES

[1] L. Wang, M. Greenspan, and R. Ellis, "Validation of bone segmentation and improved 3-D registration using contour coherence in CT data," *IEEE Trans. Med. Imag.*, vol. 25, pp. 324-334, 2006.

[2] R. Robb, D. Hanson, R. Karwoski, A. Larson, E. Workman, and M. Stacy, "Analyze: a comprehensive, operator- interactive software package for multidimensional medical image display and analysis," *Comput. Med. Imaging Graph.*, vol. 13, pp. 433-454, 1989.

[3] W. Schroeder, L. Avila, and W. Hoffman, "Visualizing with VTK: a tutorial," *IEEE Comput. Graph. Appl.*, vol. 20, pp. 20-27, 2000.

[4] T. Yoo and M. Ackerman, "Open source software for medical image processing and visualization," *Commun. ACM*, vol. 48, pp. 55-59, 2005.

[5] T. Sebastian, H. Tek, J. Crisco, and B. Kimia, "Segmentation of carpal bones from CT images using skeletally coupled deformable models," *Medical Image Analysis*, vol. 7, pp. 21-45, 2003.

[6] M. Kass, A. Witkin, and D. Terzopoulos, "Snakes: active contour models," *Int. J. Comput.* Vis., vol. 1, no. 4, pp. 321-331, 1988.

[7] L. Cohen and I.Cohen, "Finite element methods for active contour models and balloons for 2D and 3D images," *IEEE Trans. Patt. Anal. Mach. Intell.*, vol. 15, no. 11, pp. 1131-1147, 1993.

[8] C. Xu and J. Prince, "Snakes, shapes, and gradient vector flow," *IEEE Trans. Image Proc.*, vol. 7, pp. 359-369, 1998.

[9] Caselles, F. Catte, T. Coll, and F. Dibos, "A geometric model for active contours in image processing," *Numerische Mathematik*, vol. 66, pp. 1-31, 1993.

[10] V. Caselles, R. Kimmel, and G. Sapiro, "Geodesic active contours," *Int. J. Comp.* Vis., vol. 22, pp. 61-79, 1997.

[11] N. Paragios, O.M-Gottardo, and V. Ramesh, "Gradient vector flow fast geometric active contours," *IEEE Trans. Patt. Anal. Mach. Intell.*, vol. 26, pp. 402-407, 2004.

[12] L. Vese and T. Chan, "A multiphase level set framework for image segmentation using Mumford and Shah model," *Int. J. Comp. Vis.*, vol. 50, no. 3, pp. 271-293, 2002.

[13] J. Sethian, *Level Set Methods - Evolving Interface in Geometry*, computer vision, New York, USA: Cambridge University Press, 1996.

[14] S. Osher and J. A. Sethian, "Fronts propagating with curvature dependent speed: algorithms based on Hamilton-Jacobi formulations," *J. Comp. Physics*, vol. 79, pp. 12-49, 1998.

[15] C. S. Poon and M. Braun, "Image segmentation by a deformable contour model incorporating region analysis," *Phys. Med. Biol.*, vol. 42, pp. 1833-1841, 1997.

[16] X. M. Pardo, M. J. Carreira, A. Mosquera, and D. Cabello, "A snake for CT image segmentation integrating region and edge information," *Image Vis. Comput.*, vol. 19, pp. 461-475, 2001.

[17] L. Ballerini and L. Bocchi, "Multiple genetic snakes for bone segmentation," *in Applications of Evolutionary Computing: EvoWorkshops, LNCS,* vol. 2611, 2003, pp. 346-356.

[18] R. Malladi, J. A. Sethian, and B. C. Vemuri, "Shape modeling with front propagation: a level set approach," I*EEE Trans. Patt. Anal. Mach. Intell.*, vol. 17, no. 2, pp. 158-175, 1995.

[19] G. Sapiro and A. Tannenbaum, "Affine invariant scale-space," *Int. J. Comp. Vis.*, vol. 11, no. 1, pp. 25-44, 1993.

[20] A. Yezzi, S. Kichenassamy, A. Kumar, P. Olver, and A. Tannenbaum, "A geometric snake model for segmentation of medical imagery," *IEEE Trans. Med. Imag.*, vol. 16, pp. 199-209, 1997.

[21] T. Chan and L. Vese, "Active contours without edges," *IEEE Trans. Image Proc.*, vol. 10, pp. 266-277, 2001.

[22] D. Mumford and J.Shah, "Optimal approximation by piecewise smooth functions and associated variational problems," *Commun. Pure Appl. Math.*,vol. 42, pp. 577-685, 1989.

[23] M. Loog and B. van Ginneken, "Segmentation of the posterior ribs in chest radiographs using iterated contextual pixel classification," *IEEE Trans. Med. Imag.*, vol. 25, no. 5, pp. 602-611, 2006.